

On the use of machine learning algorithms in the measurement of stellar magnetic fields

J.C. Ramírez Vélez¹, C. Yáñez Márquez², and J.P. Córdova Barbosa³

¹ Instituto de Astronomía - Universidad Nacional Autónoma de México, Apdo. Postal 877, 22860, Ensenada B.C., México, e-mail: jramirez@astro.unam.mx

² Laboratorio de Cómputo Inteligente - Instituto Politécnico Nacional, Av. Juan de Dios Bátiz s/n, CP 07738, CDMX, México.

³ CUCEA, Universidad de Guadalajara, Periférico Norte 799, Los Belenes, Zapopan Jalisco, 45100, México.

ABSTRACT

Context. Regression methods based in Machine Learning Algorithms (MLA) have become an important tool for data analysis in many different disciplines.

Aims. In this work, we use MLA in an astrophysical context; our goal is to measure the mean longitudinal magnetic field in stars (H_{eff}) from polarized spectra of high resolution, through the inversion of the so-called multi-line profiles.

Methods. Using synthetic data, we tested the performance of our technique considering different noise levels: In an ideal scenario of noise-free multi-line profiles, the inversion results are excellent; however, the accuracy of the inversions diminish considerably when noise is taken into account. In consequence, we propose a data pre-process in order to reduce the noise impact, which consists in a denoising profile process combined with an iterative inversion methodology.

Results. Applying this data pre-process, we have found a considerable improvement of the inversions results, allowing to estimate the errors associated to the measurements of stellar magnetic fields at different noise levels.

Conclusions. We have successfully applied our data analysis technique to two different stars, attaining by first time the measurement of H_{eff} from multi-line profiles beyond the condition of line autosimilarity assumed by other techniques.

Key words. Atmospheric magnetic fields; Line: formation profiles; Polarized radiative transfer; Stars: HD 190771, HD 9472

1. Introduction

Magnetic fields are a key ingredient in the study of the stellar evolution and yet many of their aspects are still unknown, among other reasons, due to the difficulty to detect, measure and map (whenever this is possible) surface magnetic fields in stars other than the Sun.

Nonetheless, a lot of progress has been made in the recent years in the study and observation of stellar magnetic fields, and some facts are now well-established. For example, non chemically peculiar massive stars can host stable strong dipolar configurations and the mean longitudinal magnetic fields (H_{eff}) for these stars vary from tens to thousands of gauss (e.g. Donati & Landstreet 2009; Wade et al. 2016; Grunhut et al. 2017); or that the solar type stars during the main sequence phase, harbor more complex magnetic geometries and exhibit much weaker effective fields (H_{eff}), by at least one order of magnitude, namely, in the order of tens of gauss or less (e.g. Petit et al. 2008; Marsden et al. 2014). These two examples are of interest for this work from a data analysis point of view, because their results were obtained using the so-called multi-lines approach. This means that to retrieve a signal in the circular polarised Stokes parameter (V), in order to detect and to subsequently measure the magnetic field, it is necessary to co-add as many as possible individual spectral lines. The line addition permits to boost the signal-to-noise ratio value in the resulting “mean” circular profile. Otherwise, the individual V profiles are in general systematically below the noise level.

The underlying idea of grouping many lines together into a single one is that the noise addition is incoherent while the addition of the V profiles is coherent (Semel & Li 1996), i.e., the more individual profiles are co-added, the better signal to noise ratio is retrieved in the mean profile. Typically, an ad-hoc selection of unblended lines is performed establishing a linear relation between the mean circular profile and the mean longitudinal magnetic field. The number of lines to combine depends on the spectral type of the star and on the instrumental resolution. In the case of modern high resolution spectroplarmeters such as HARPS, ESPaDOnS or NARVAL, the total number can reach up to ten thousand lines, or more, for late-type stars.

Different techniques have been proposed to perform the line addition, and they can be roughly divided into two groups: 1) the line addition is based on the assumption that all the lines are autosimilars (e.g. Donati et al. 1997; Wade et al. 2000; Kochukhov et al. 2010) or apply deblending process to extend the range of applicability of the technique (Sennhauser et al. 2009; Sennhauser & Berdyugina 2010) and 2) the line autosimilarity assumption is not necessary (e.g. Semel et al. 2006, 2009; Ramírez Vélez et al. 2010). The mean profiles obtained in the former approach are called Least-Square-Deconvolved (LSD) profiles after the work of Donati et al. (1997), and they require the use of unblended lines, while the mean profiles issued from the latter approach are called Multi-Zeeman-Signatures (MZS) after the work of Semel et al. (2009), and in this case the mean profiles are established including blended and unblended lines.

For the LSD profiles, the measurement of the strength of the mean longitudinal magnetic fields can be done through the weak field approximation (WFA, see e.g. Jefferies et al. 1989), or

Send offprint requests to: jramirez@astro.unam.mx

alternatively, with the centre-of-gravity method (COG, see e.g. Rees & Semel 1979) through the first-order moment of the mean circular profile (Mathys 1989). The employment of the WFA and of the COG methods are of great utility because they allow to measure the effective magnetic field without having to recourse to radiative transfer calculations. Nowadays, the COG method is the technique used by excellence to determine H_{eff} from the LSD profiles. Nevertheless, both approaches have limitations due to assumption of self-similarity of the lines, having to fulfill simultaneously both conditions: the use of unblended lines and the measurement of *weak* magnetic fields. The range of application in the data analysis is thus difficult to determine precisely. For example, concerning the second condition related to the strength of the magnetic fields, Kochukhov et al. (2010) stated a maximum of 2 kG as limit for the analysis of circular polarised LSD profiles; however, as noticed by Carroll & Strassmeier (2014) the limit of the WFA of local profiles, i.e. to reach the Zeeman saturation regime in individual lines, is around one kG for lines in the optical wavelength range. In any case, to bypass the inherent limitations associated to the use of the LSD profiles and to dispose of a more general approach, in this work we continue developing a method based in the analysis of the MZS profiles.

In a previous work, Ramírez Vélez et al. (2016, hereafter Paper I), we presented a new inversion code for the measurement of stellar magnetic fields using a complete radiative transfer approach. We used as case of study a solar type star ($T_{\text{eff}} = 5500\text{ K}$), to show that the MZSs can be used to correctly retrieve the stellar longitudinal magnetic field in cool stars. The proposed methodology illustrates that it is feasible to infer H_{eff} , in the context of the multi-lines approach, beyond the assumption of lines autosimilarity, i.e. beyond the employment of the COG method (or the WFA).

The inversion code used in Paper I was based on a look-up table, i.e. the higher the number of stellar MZSs contained in the table the better were the results obtained. This fact makes of our technique a very CPU-time consuming method. In this work we incorporate the use of machine learning algorithms to remarkably decrease the number of synthetic stellar spectra required to properly determine H_{eff} .

In section II, we show the performance of different machine learning algorithms for the inversion of ideal noiseless MZSs, to subsequently show that the effectivity of the regression algorithms is strongly affected when noise is included, even for very small noise levels. In section III we incorporate pre-process data analysis to reduce the noise effect when inferring H_{eff} . In section IV we apply our method to two real cases and compare our results to previous ones published in others studies, to finally draw some general conclusions in section V.

2. The machine learning strategy

In the stellar physics domain, the number of published studies using analysis methods based in machine learning algorithms has been growing, specially in the last years, either for classification of stars (e.g. Richards et al. 2011; Armstrong et al. 2016) or in the search of exoplanets (e.g. Davies et al. 2016), or in the determination of stellar fundamental parameters (e.g. Bellinger et al. 2016; Verma et al. 2016; Angelou et al. 2017), among many others. In this work we will use the machine learning approach in the context of the study of stellar magnetic fields.

As previously mentioned, in Paper I we performed inversions of MZSs using a code based in a look-up table strategy, meaning that given a MZSs to invert we find as solution the closest-norm

MZSs in the table. The MZSs were constructed adopting the eccentric tilted dipole model (Stift 1975). In this model, we considered as free: 1) all the parameters that describe the magnetic geometry of the dipolar configuration (the three Eulerian angles α, β, γ , and the inclination angle (i) of the stellar rotation axis respect to the line of sight), 2) the position of the magnetic dipole inside of the star given by two coordinates (X_2, X_3), and 3) the strength of the dipolar moment (m), leading to a total of 7 free parameters. It turned out that in order to obtain good enough inversion results, it was required to calculate 7500 stellar spectra models. For each synthetic spectrum we randomly varied the 7 free parameters, covering a spectral range from 350 to 1000 nm, giving a total close to 350000 wavelength points per spectra. This huge number of thousands of stellar spectra, required to shape the table, demands a lot of computer calculation time which damps the employment of our technique for the analysis of big databases, such as *Polarbase*¹ (Petit et al. 2014), where hundreds of observed spectra of cool stars can be found.

To reduce the required number of stellar spectra to invert the MZSs, in this work we implemented 3 different regression methods based in machine learning algorithms. All these three regression models belong to the supervised paradigm and are included in the *Scikit-learn* software package (Pedregosa et al. 2011) of the Python language. The employed regressions are: 1) The Bayesian Ridge Linear Regression (BR), 2) The Support Vector Machine (SVM), and 3) The Multi Layer Perceptron Artificial Neuronal Network (ANN). We next briefly describe each one.

Regression analysis is a valuable mechanism to model and analyse data, constituting a form of predictive modelling technique used to explore the relationship between two (or more) variables: an independent one, the input (also known as feature or predictor), and a dependent one, the target. Its goal is to fit a curve to the data points in such a form that the sum of differences between the data points and the curve is minimal (e.g. Tan et al. 2005). We next briefly describe each of the regressor models employed in this work.

2.1. Bayesian Ridge

Linear Regression is one of the most frequently used modeling techniques: It establishes a linear relationship between the dependent variable (y) and one or more independent variables (x):

$$y(\mathbf{x}, \mathbf{w}) = w_0 + w_1x_1 + w_2x_2 + \dots + w_nx_n, \quad (1)$$

where the coefficients w_i are known as the parameters of the regression model. The first coefficient w_0 is the so-called intercept or “bias” of the model. In our case, the input variable are the MZSs and the target can be any parameter of either the stellar atmospheric model or the magnetic model (as for example T_{eff} or H_{eff}).

The linear model that best fits the data is commonly calculated using the Least Square Method and when this is the case, the performance of the calculated model is measured by the R-square metric (Glantz et al. 2016). It is important to notice that this kind of regression require that a linear relationship between both independent and dependent variables exists. It is also noteworthy the fact that outliers terribly affect the regression line and, therefore, the estimated values.

If the power of the predictor on the estimated regression equation is bigger than one, then the regression is known as poly-

¹ <http://polarbase.irap.omp.eu/>

nomial. In that case, the regression line is not a straight line but a curve that fits to the points. A higher power on the independent variable allows a better fit for more complex datasets.

However, when the data experiences from multicollinearity, meaning that it has multiple, highly correlated predictors, then the Ridge Regression technique is used. When multicollinearity occurs, the Least Squares estimates are unbiased but the variances are large, which in turn results on a higher error on the predicted values. To correct this error, Ridge Regression adds a bias to the regression estimates and it solves the multicollinearity problem through a shrinkage parameter λ :

$$\min \|y - \mathbf{x}\mathbf{w}\|_2^2 + \lambda \|\mathbf{w}\|_2^2 \quad (2)$$

The shrinkage parameter, $\lambda \geq 0$, penalizes the size of the coefficients on the original equation and it is the direct regulator of the amount of shrinkage, a process also known as regularization (e.g. Yang & Zou 2015).

The regularization of the parameters, can be done using the Bayesian Regression technique: it introduces diffuse priors, also known as noninformative priors, which are probability distributions expressing general information. Using the Bayesian approach, the regularization of the Ridge Regression model is equivalent to finding a maximum solution for a Gaussian prior (the previously mentioned diffuse prior) with precision λ^{-1} . However, instead of setting lambda manually, it is possible to consider it as a random variable to be estimated from the data if the predicted output y is assumed to follow a Gaussian distribution around $\mathbf{x}\mathbf{w}$:

$$p(y|\mathbf{x}, \mathbf{w}, \alpha) = N(y|\mathbf{x}\mathbf{w}, \alpha), \quad (3)$$

where α is a random variable and it needs to be estimated from the dataset. A particular case of Bayesian Regression is the Bayesian Ridge Regression, where the prior for the parameter ω is given by a spherical Gaussian distribution, as in:

$$p(\omega|\lambda) = N(\omega|0, \lambda^{-1}\mathbf{I}), \quad (4)$$

where \mathbf{I} is the identity matrix. It is during the fit of the model that the set of parameters ω, λ, α are estimated jointly (Carlin & Louis 2008; Pedregosa et al. 2011).

2.2. Support Vector Machines

Support Vector Machines is a learning method used mostly to classify data and to detect outliers, but it can also be used for regression purposes. The SVM offers important characteristics in his performance, as for example high effectiveness in high dimensional spaces, usefulness even when the number of samples is lower than the number of dimensions and the memory efficiency. In the SVM approach, data is plotted as points in a n -dimensional space and the outcome of the algorithm will be an optimal hyperplane that best categorizes the data classes (for classification purposes) or best predict the tendency of the data in order to predict future unknown data (regression model) (e.g. Du & Swamy 2014; García-Florian et al. 2018).

In the specialized literature, two main modalities are reported to perform regression tasks through the use of the SVM model, which are: the ϵ -support vector regression (ϵ -SVR) and the ν -support vector regression (ν -SVR), Vapnik (1999). In this work we have used the former approach ϵ -SVR: Let $\mathbf{X} = (\mathbf{x}_1, \mathbf{x}_2, \dots, \mathbf{x}_m)$

be a set of observations of the same independent variable, and let $\mathbf{y} = (y_1, y_2, \dots, y_m)$ the corresponding dependent variables. Also, let \mathbf{w} be the weight vector, let b be a scalar, let $\Phi(\mathbf{x})$ be a non-linear function, let ξ_i be slack variables, and let $C > 0$ be their associated parameter. If $\epsilon > 0$ is the associated parameter with the ϵ -insensitive loss function, the ϵ -SVR solves the following optimization problem:

$$\min_{\mathbf{w}, b, \xi, \xi^*} \frac{1}{2} \mathbf{w}^T \mathbf{w} + C \sum_{i=1}^m \xi_i + C \sum_{i=1}^m \xi_i^*, \quad (5)$$

subject to

$$\begin{aligned} \mathbf{w}^T \Phi(\mathbf{x}_i) + b - y_i &\leq \epsilon + \xi_i, \\ y_i - \mathbf{w}^T \Phi(\mathbf{x}_i) - b &\leq \epsilon + \xi_i^*, \\ \xi_i, \xi_i^* &\geq 0, i = 1, \dots, m. \end{aligned} \quad (6)$$

Similarly, the dual problem is defined according to α :

$$\min_{\alpha, \alpha^*} \frac{1}{2} (\alpha - \alpha^*)^T - Q(\alpha - \alpha^*) \quad (7)$$

subject to

$$\begin{aligned} \mathbf{e}^T (\alpha - \alpha^*) &= 0 \\ 0 \leq \alpha_i, \alpha_i^* &\leq C, i = 1, \dots, m \end{aligned} \quad (8)$$

where the \mathbf{e}^T is the identity vector and $Q_{ij} = K(\mathbf{x}_i, \mathbf{x}_j) \equiv \Phi(\mathbf{x})^T \Phi(\mathbf{x})$ is the kernel function, which can be linear, polynomial, sigmoid or a radial basis function, among other options. The dual problem is solved by the Lagrange multipliers, and the resulting function is (Chang & Lin 2011):

$$f(\mathbf{x}) = \sum_{i=1}^m (-\alpha_i + -\alpha_i^*) K(\mathbf{x}_i, \mathbf{x}_j) + b. \quad (9)$$

In our case, i.e. data analysis of MZSSs, we found after testing different kernel functions that it was with the linear function that we obtained the best predictions results.

2.3. Artificial Neuronal Network

Artificial neural networks are inspired by physiological knowledge of the organization of the brain. They are structured as a set of interconnected identical units known as artificial neurons, and the interconnections are used to send signals from one neuron to the others, in either an enhanced or inhibited way. This enhancement or inhibition is obtained by adjusting connection weights. In an artificial neural network, a new observation causes an update of the network weights, which means that the network *learns*.

Let $x_i \in \mathbb{R}^n$ be the i -th observation from a set of m of them (corresponding to the same independent variable), and let $x_{ij} \in \mathbb{R}$ be the j -th value of the i -th observation. From these m values and a previously established threshold value θ , it is possible to model a simple perceptron, which is an artificial (and very effective) model of a physiological neuron (Rosenblatt 1958). It is considered that the j -th value of the i -th observation (corresponding to a dendrite of a physiological neuron) has an associated weight $w_{ij} \in [0, 1]$ when x_{ij} becomes the entrance to the central part of the neuron (which corresponds to the *soma* of the physiological counterpart). The weight with value 1 is associated with the threshold value θ .

The process that occurs in the *soma* of the artificial neuron, is what gives the power to the machine learning algorithms based on artificial neural networks. This process involves a sum of the products and a function of activation of the neuron. Each product is obtained by multiplying the value of the neuron x_{ij} with its associated weight w_{ij} while the activation function Θ is typically a sigmoid function or the tanh function. The result of this process, which is the output of the artificial neuron for of the i -th observation, is shown in the following expression:

$$\text{output}(i) = \Theta \left[\left(\sum_{j=1}^n w_{ij} x_{ij} \right) - \theta \right]. \quad (10)$$

The simple perceptron is the fundamental building block of virtually all models of artificial neural networks of the state of the art (with some singular exceptions represented by unconventional models, such as morphological and Alpha-Beta models). The choice of the ways of interconnecting the simple perceptrons gives rise to different network topologies, among which stand out, undoubtedly the models known as *fully connected layered feedforward networks*.

This type of models are organized in layers: an input layer, an output layer and one or more hidden layers. One of its important features is no connection or feedback between neurons of the same layer, but the connections, as the name implies, are all feedforward; that is, a neuron located in a certain layer, only connects with one or several neurons of the adjacent layer forward (e.g. Du & Swamy 2014).

The Multi Layer Perceptron (MLP) is a fully connected layered feedforward network that is trained with the method known as backpropagation, whose detailed description can be consulted in Rumelhart et al. (1985). The MLP can be used as a classifier or as a regressor, and in this article we use a regressor version of the MLP known as MLPRegressor, which is trained with backpropagation using identity as with the *identity* function as the activation function in the output layer, that corresponds to the output y of our application (Pedregosa et al. 2011).

2.4. Regression model parameters

In practice, the implementation of each regressor model is defined by a set of hyperparameters, as for example the activation function or the value of the penalization coefficients, etc. The choice of each hyperparameter for the three regressors used in this work are all included in Appendix A.

For the choice of the different hyperparameters in each regression model we tested the inversion effectivity by varying the values of many hyperparameters; the final values that were selected (listed in Appendix A), were those that offered better inversion performance for each regressor.

Finally, for the cases of the SVM and the ANN regressors, the associated learning algorithms are sensitive to the data distribution. Both regressors assume that the data is centred around zero and is close to a standard normal distribution. For this reason, it is required to apply a standardization of the data before the training is performed. We have thus applied a pre-process to the data prior to the training process through the *StandardScaler* utility included also in the *Scikit-learn* software package.

3. Inverting MZSs

In this section we will employ the three different regression models mentioned above to estimate the H_{eff} using a supervised train-

ing. The reason for using three different models is to determine to what extent the results depend on the choice of the model, and thus to choose the most adequate one.

3.1. Inverting noiseless MZSs

The MZSs that we will employ in this section are those previously established in Paper I, where we considered the case of a cool star adopting from the Atlas9 grid (Castelli & Kurucz 2004) an atmospheric model with $T_{\text{eff}} = 5500 \text{ K}$, $\log g = 4.0$, solar metallicity, zero macro-turbulence ($v_{\text{turb}} = 0.0$) and a micro-turbulent velocity of $\xi = 2.0 \text{ km s}^{-1}$. Besides, we considered a slow rotator case fixing $v \sin i = 10 \text{ km s}^{-1}$. For the synthesis of the Stokes profiles we employed the code COSSAM (Stift 2000; Stift et al. 2012). All the atmospheric parameters were kept fixed, but we allowed to randomly vary the 7 parameters that describe the configuration the dipolar tilted eccentric model (see above). The inversions showed that none of the free parameters could be retrieved being only possible to infer H_{eff} . The fact that none of the free parameters of the dipolar model could be retrieved is due to the existent degeneracy among different combinations of parameters that can produce the same observable: H_{eff} (see Fig. 10 in Paper I). For this reason, the machine learning algorithms will be trained to predict only one target, the H_{eff} . We point out that our goal is to measure the stellar longitudinal magnetid field from spectropolarimetric snapshot data type, and not to map the strength of magnetic field over the surface.

As first step, we must determine the (small enough) number of MZSs that we will use to train the regression models, keeping in mind that it is required to obtain satisfactory and acceptable predictions (inversion results).

For this purpose, we first used only 50 MZSs to train the algorithms and then we tested each regression model inverting a representative set of 1500 MZSs. We then repeated the exercise but increasing the number of MZSs used in the training process by steps of 50 until reach a maximum of 500. The performance for all the regression models is shown in Fig. 1. The three models showed similar results, obtaining very accurate determinations of the H_{eff} even when we considered a very small number of MZSs in the training process: using 100 MZSs the obtained RMSE is inferior to 1 gauss. The general tendency is that the errors decrease smoothly as we increase the number of MZSs employed in the training. Based in these results, we have decided that training the algorithms with 300 MZSs is sufficient for a proper determination of the stellar longitudinal magnetic field. Thus, hereafter all the inversions tests will be performed using 300 MZSs in the training process. In Fig. 2 we show the individual inversions of the 1500 MZSs for the three regression models.

The excellent results of Fig. 2 show the great utility of the employment of machine learning algorithms in the inference of H_{eff} from the MZSs. As comparison, in Paper I we constructed 7500 spectra models and the RMSE of those inversions was 3.95 G, while with the best regression model (BR) we now obtain a RMSE of 0.41 G requiring only 300 spectra models. In other words, using this regression model the inversions accuracy is increased by one order of magnitude, and at same time the required time to synthesize the stellar spectra models (number of MZSs) is reduced by a factor of 25. It is important to remark that the required time for the training of the algorithms is very fast: using a single processor the cpu-time required was of 1, 5 and 120 seconds for the BR, SVM and ANN regressors respectively; moreover, in the case of BR and the ANN the time can be reduced since the training process be parallelized.

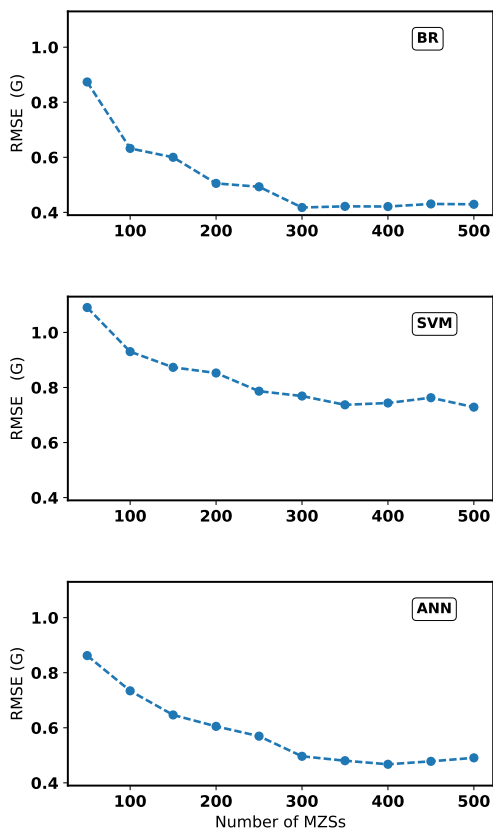


Fig. 1. Root mean square inversions errors (RMSE), in units of gauss, as function of the number of MZSs included in the training; the inner legend in each panel indicates the employed regression model (see text for details). The inversion sample consist of 1 500 MZSs.

Unfortunately, the effectivity of the regression models is considerably reduced when noise is taken to account. To illustrate this, we repeat the same exercise of Fig. 2 but this time including 5 different noise levels in the MZSs. The noise level, see Fig. 3, is quantified as the standard deviation of the noise divided by the standard deviation of the noise-free MZSs. In Fig. 4 we show the inversion results only for the BR model, which was the best regressor for the case of ideal MZSs without noise. (We note that our definition of noise level is consistent with the work of Carroll & Strassmeier (2014), so we can latter on make a proper comparison of the results.)

From the results of Fig. 4, it is clear that for the inversion of noise-affected MZSs, the case corresponding to real data, the predictions are no longer good enough, even for the lowest noise level. For these tests, the training process was performed using noise-affected MZSs (with their respective noise levels), because in the contrary case – training with noiseless MZSs–, the errors were even slightly higher. Besides, it is also worth noticing that we have verified that the number of MZSs to include in the training process does not depend on the noise levels, i.e., to consider 300 MZSs in the training process is good enough for all noise levels.

Based on the obtained results when noise is included, we propose a two steps process to improve the efficiency of the MZSs inversions. These two steps consist in a MZSs noise-cleaning and in an iterative inversion methodology.

3.2. Denoising profiles with PCA

To facilitate the analysis of observed data, it is desirable to dispose of some noise treatment in order to give more credibility to the results. In the case of stellar spectropolarimetric data, the establishment of the multi-line (LSD or MZS) profiles is already a pre-processing step of the data analysis. However, the multi-line profiles are also affected with noise, which in turn degradate the accuracy of the inversions. Thus, we will subsequently refer as *noise treatment* to any process applied to the multi-line profiles in order to deal with the noise problem.

Noise treatment, in this sense, can be implemented using for example any of two following approaches. On the one hand, the sparsity representation of data samples has recently begun to be implemented in the analysis of solar and stellar spectropolarimetric data with very good results (Asensio Ramos & de la Cruz Rodríguez 2015; Carroll & Strassmeier 2014). On the other hand, the principal components analysis (PCA), first introduced by Rees et al. (2000) for the study of solar magnetic fields, is a more commonly employed technique in the analysis of both, solar and stellar spectropolarimetric data. Both approaches implement a sort of space dimensionality reduction allowing to diminish the impact of the noise in the retrieval of the model parameters.

We will employ PCA to perform a “noise-cleaning” of the MZSs: In the previous section we decided to use 300 MZSs for the training of the regression algorithms. Applying the Singular Value Decomposition to this same set of MZSs we obtain in turn 300 eigenvectors. It is well known that the eigenvectors are a mathematical base of the original set of MZSs, such that any MZSs can be obtained as a linear combination of those eigenvectors (e.g. Golub & van Loan 1996). Nevertheless, it is also possible to consider not the entire set of eigenvectors but only the first ones, because in fact the first eigenvectors are those that contain most of the usefull information about the original MZSs (e.g. Paletou 2012). Accordingly, we considered only the first ten eigenvectors to perform a noise-cleaning:

$$MZS_{\text{cleaned}} \equiv \sum_{i=1}^{10} \alpha_i ev_i, \quad (11)$$

where α_i denote the scalar coefficients and ev_i the eigenvectors. The coefficients can be obtained through a dot product between each eigenvector and the MZS.

In Fig. 3, we illustrate the cleaning proces of MZS profiles considering the same 5 levels of noise previously used (from 0.2 to 1.0 in steps of 0.2). The solid lines in the upper panels correspond the noise added profiles, while in the lower panels they represent the respective cleaned profiles. As comparison, the dashed lines in both, upper and lower panels, correspond to the original noise-free profiles. It can be noticed that the noise cleaning process works well even for the highest noise level. However, as expected, the higher the noise level, the greater the difference between the original and the cleaned MZSs are found.

We applied the described process to the full set of 1500 MZSs and repeated the same inversion test of Fig. 4, but this time implementing a noise cleaning prior to the inversion of the profiles. Surprisingly, the results are not as good as expected, being only slightly better to the case without cleaning process, as shown in Table 1. For this reason, we propose a complementary step in the data analysis to improve the inversion efficiency.

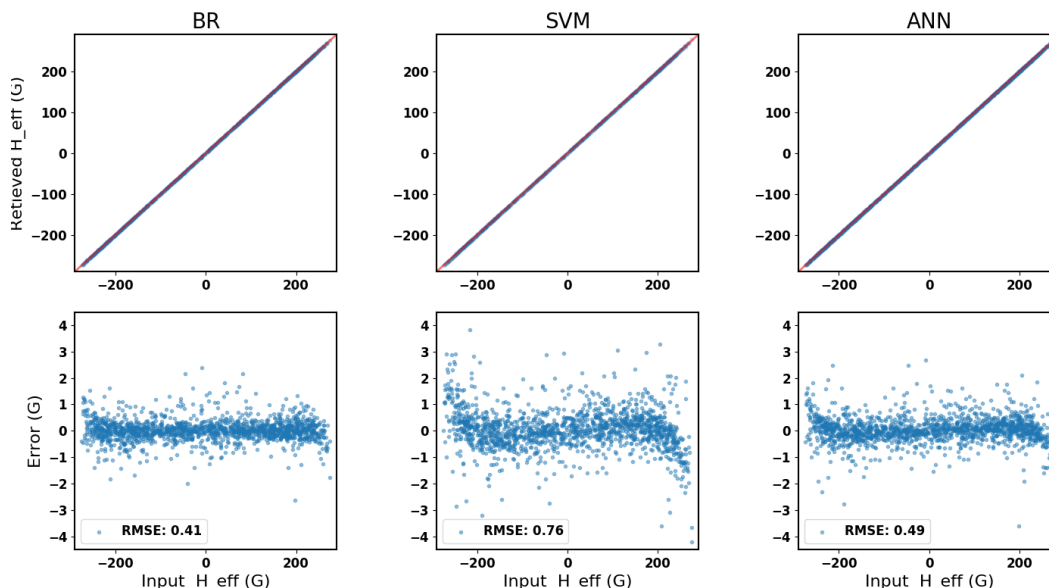


Fig. 2. Performance of the regression models when 300 MZSs were considered during the training process. The X axis for all panels corresponds to the original value of H_{eff} for each of the 1 500 MZSs. In the upper panels the Y axis represents the predicted values of the inversions, while in the lower panel it corresponds to the inversion errors in units of gauss. The red line in the upper panels represents a one-to-one relation.

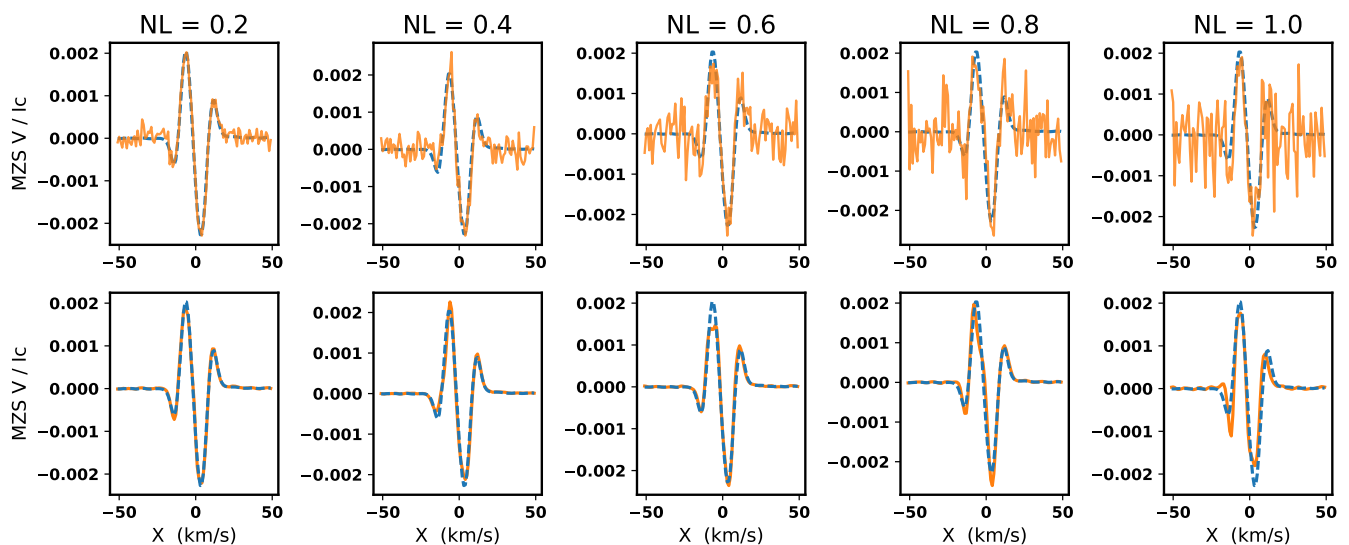


Fig. 3. In both, upper and lower panels, the dashed line represents the original (noiseless) MZSs. The solid line in the upper panels corresponds to the noise added MZSs; on top of each column are indicated the levels of noise. In the lower panels, the solid lines represent the cleaned MZSs.

Table 1. Comparison of the RMSE for inversions performed considering a noise cleaning process of the profiles and when not. The employed regressor model was the BR.

	Noise Level					Cleaned
	0.2	0.4	0.6	0.8	1.0	
RMSE (G)	14.0	24.6	32.2	37.2	44.5	No
RMSE (G)	13.2	24.0	26.9	34.5	39.2	Yes

3.3. Iterative inversion process

Let us consider only one given MZS from which we would like to infer H_{eff} , and let us also consider a given fixed noise level, for example 0.4. In the previous section we showed how to perform a noise cleaning of the profiles. We consider now a scenario in which we could repeat this process several times. For each iteration, the random noise will affect differently the MZS and subsequently the noise cleaned profiles will all be slightly different. In Fig. 5 we illustrate how the cleaned profiles at each iteration differ from the original noise-free profile. For example, the maximum amplitude for the bottom left cleaned profile is higher than the original one, contrary to the bottom central cleaned profile where the maximum amplitude is inferior to the original

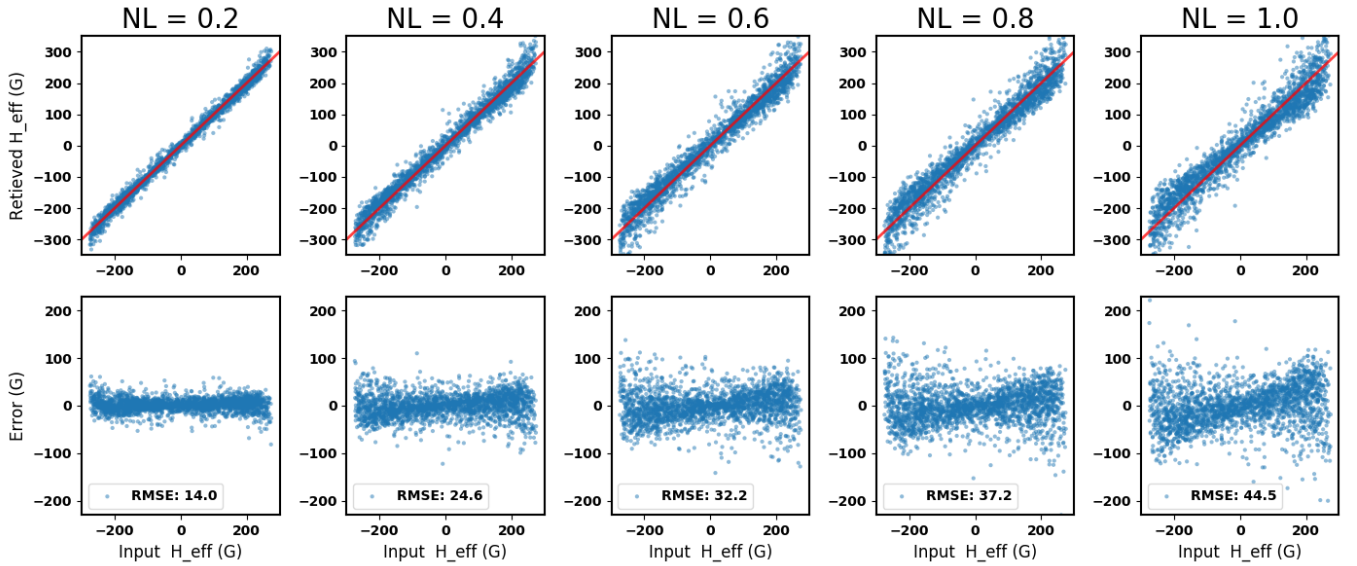


Fig. 4. Inversions of noise-added MZSs using the BR model. The different noise levels (NL) added to the MZSs are indicated in top of the upper panels. The X and Y axes are the same as in Fig. 2 .

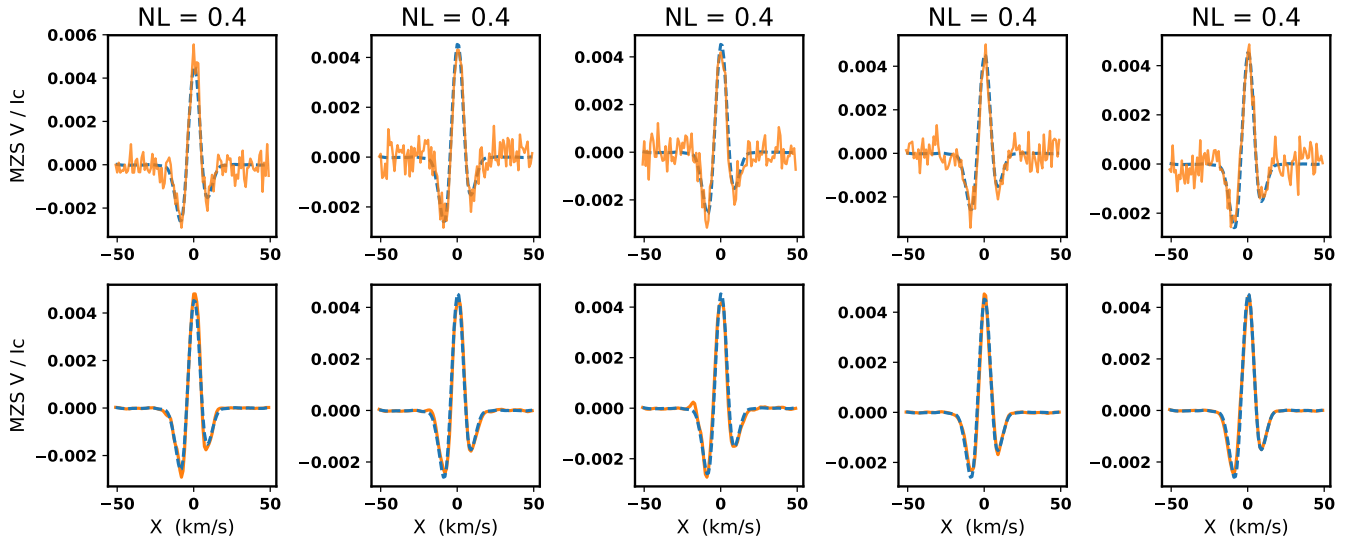


Fig. 5. Iterating the cleaning process considering one given MZSs and the same noise level. The solid and dashed lines represent the same as in Fig. 3. As shown in bottom panels, at each iteration the cleaned profiles show small but different deviations from the original noiseless profile.

one. These differences, even if very small, are enough to produce a different result when inferring the longitudinal magnetic field. Nevertheless, we know that all the cleaned profiles have the same origin in the sense that all were established from the same noiseless data (dashed lines in Fig. 5). It is thus expected that the inversions derived from these cleaned profiles will be close to the real value of H_{eff} , and in fact they are, showing a distribution centred around the original value of H_{eff} .

To illustrate our proposed methodology, in Fig. 6 we show two examples of iterative inversions. We have considered two MZSs, one with an H_{eff} of 238.2 G (left panels) and one with a much weaker magnetic longitudinal field of 5.2 G (right panels). From top to bottom, the three panels show how the inversion distributions varies with the number of iterations: the larger the number of iterations performed, the more the histograms will

approximate a normal Gaussian distribution (solid line in black). The centroid of the fitted Gaussian distribution, indicated with a vertical line, corresponds to the inferred value of H_{eff} in each histogram.

In order to inspect more carefully the dependence of the results on the number of iterations, we tested the proposed inversion process using the full set of 1 500 MZSs. Additionally, it is interesting to compare the performance of the three regression models introduced above. We recall that we are considering the same noise level of 0.4 for all the iterations and for all the MZSs. The RMSE of the inversions for the full set of profiles as function of the number of iterations is shown in Fig. 7. All the three regressor models show very similar behaviors, with a considerable improvement of the results specially for the first hundreds iterations: When no iteration is applied the RMSE are 24.6, 29.7

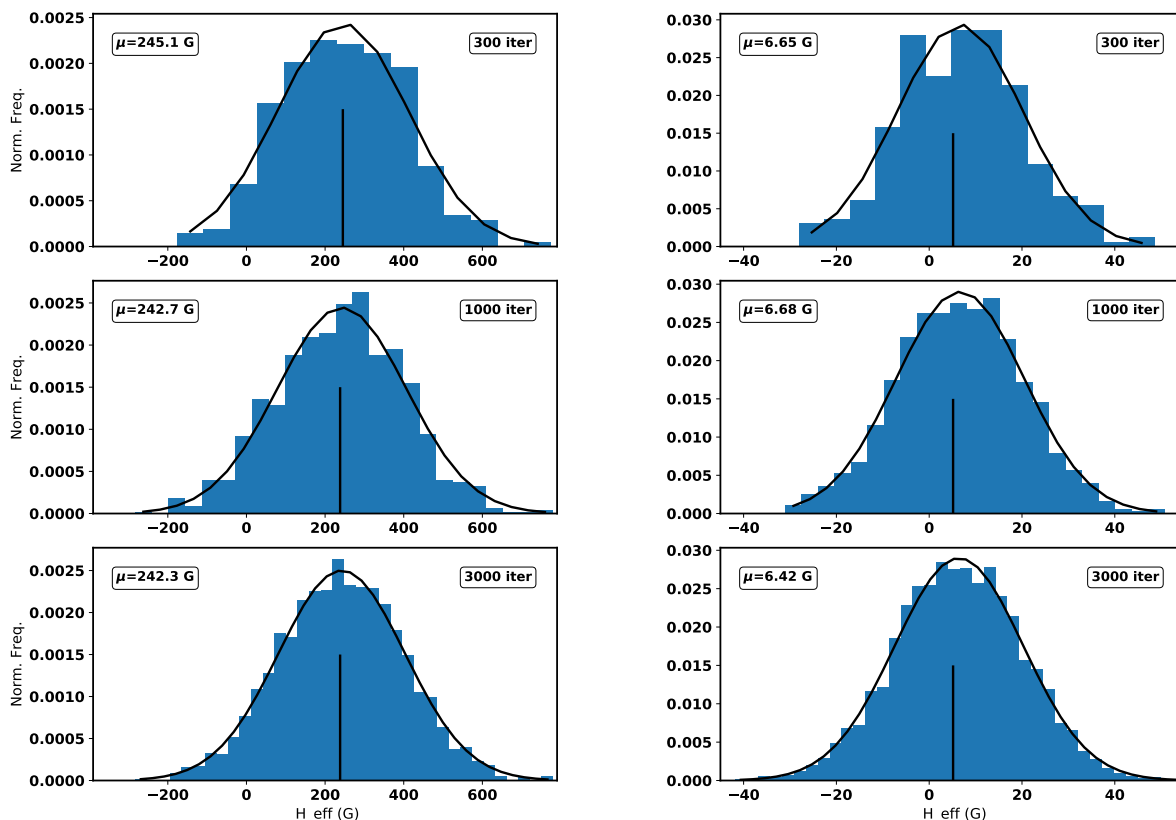


Fig. 6. Two examples of the iterative inversion process; the original values of H_{eff} are 238.2 G (left panels) and 5.2 G (right panels). Each histogram shows the inversion distributions considering different numbers of iterations (indicated in the upper right corner). The upper left legend in each histogram indicates the centroid of the fitted normal Gaussian distribution, which would correspond to the inferred value of H_{eff} in each case.

and 26.3 G for the BR, SVM, and ANN respectively, and after 100 iterations the RMSE is reduced to 16 G for the three models, and at 1000 iterations the RMSE is of only 6 G. After around one thousand iterations, the improvement of the inversions becomes restrained. With the present results, we consider that apply 3000 iterations is good enough for the adopted inversion strategy.

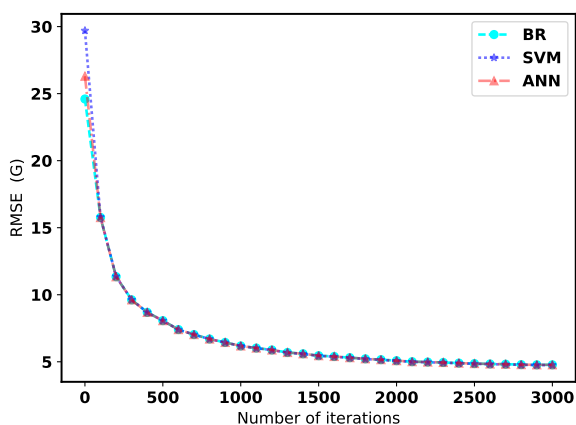


Fig. 7. Performance comparison of the three regression models as function of the number of iterations when considering noise level of 0.4. The performance of the three regressor is almost identical.

Now, concerning the incertitudes associated to our measurements of H_{eff} , in principle, it is possible obtain an error esti-

mation based in the the histograms of Fig. 6. Nevertheless, by doing it we would be highly overestimating the errors: The standard deviation of the fitted Gaussian distribution for the bottom left panel is 160 G, but in fact the error is much more smaller, being of only 4.1 G. Similarly, an overestimation of the error is also obtained in other example of Fig. 6, at bottom right panel, where the standard deviation of the fitted distribution is 13.8 G but the real error is of only 1.2 G. Thus, in order to obtain realistic estimations of the errors, we next proceed to inspect the inversions over the full sample of 1500 MZS.

3.4. Characterizing the technique

We will now show the performance of our proposed method considering different noise levels; we tested the inversions using the same set of 1500 MZSs as before, and in all cases we applied 3000 iterations. To quantify the accuracy in the results we have employed the Mean Absolute Percentual Error (MAPE), defined as:

$$MAPE = 100 * \left(\frac{|H_{\text{eff}}^{\text{original}} - H_{\text{eff}}^{\text{inferred}}|}{|H_{\text{eff}}^{\text{original}}|} \right). \quad (12)$$

Additionally, in order to underline the importance of including a noise treatment in the analysis of spectropolarimetric data, which in our case is done through the noise cleaning of the MZSs followed by the iterative inversion procedure, we also included the results when the profiles were inverted without any noise treatment, which we labelled as *single* inversions.

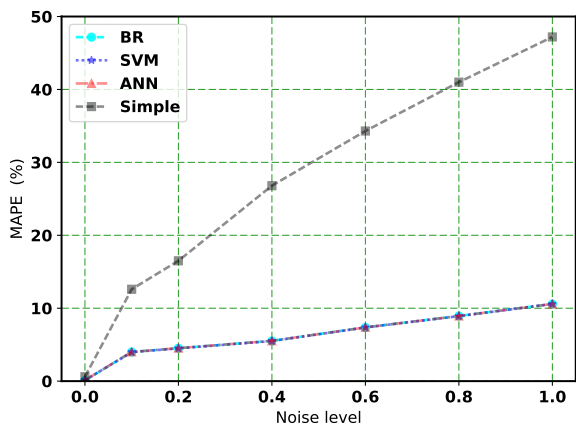


Fig. 8. Response of the MAPE of the inversions considering different noise levels. Each of the three regression models, as well as the case of *single* inversions, are indicated in the inner legends.

In Fig. 8, we show the variation of MAPE as function of the noise level. The three regressor models (BR, SVM, ANNN) have the same performance as function of the noise level: When no noise is included the MAPE is extremely low (0.1%), but the inclusion of even a very small noise level of 0.1 lead to a (relative) considerable increment of the MAPE (4%). However, the precision of the inversions for the models will then only decrease moderately to finish with a MAPE of 11% for the highest noise level of 1. Finally, the case of traditional inversions –noted *simple* by the line with square symbols–, is the most affected one, varying from 13% for the lowest noise level of 0.1 up to 47% for the highest noise level of 1.

One conclusion from this test is that with our proposed methodology –PCA noise cleaning combined with iterative inversions–, the three regression models are robust methods to determine H_{eff} from MZSs that are affected by the noise. Another important conclusion is that the *single* inversions are highly affected by noise, being the respective errors much higher than those obtained with any of the regression models. This is particularly evident for the case of highest noise level of unity, where the MAPE of the *single* inversions can reach almost 50%, while for all three regressors, for this same noise level, the MAPE is close to 10%.

Similar results have been previously presented in Carroll & Strassmeier (2014). In this work the noise treatment is done adopting a *sparsity* representation of the data using an Orthogonal Match Pursuit (OMP) algorithm. In Fig. 10 of that article, the authors presented an analogous test to the one just discussed here, comparing the inversions of noise affected profiles using the OMP approach with the ones obtained using the traditional centre-of-gravity (COG) method. The latter, is nowadays the usual method employed when measuring H_{eff} from real data and it is relevant in the sense that it does not consider any noise treatment. The authors have found that when considering a noise level of 1, using the COG method the MAPE is close to 50% (the same as in our *single* case), while using the OMP approach the MAPE decreases to less than 20%. Both results, theirs and ours, stand out the importance of implementing a noise treatment in the inversion of polarised multi-line profiles.

The iterative process described in this section is a time-expensive step in our approach since it takes 3.75 hrs using 8 processors in parallel. Nevertheless this relative long time is re-

quired in order to achieve the precision errors showed in Fig. 8, and of course this time can be reduced if more processors are at disposal.

4. Applying the method to real data

4.1. HD 190771

In this section we will apply our method to real data. We have obtained from the public database *PolarBase*, spectropolarimetric data of two cool solar like stars, with very similar physical properties to the Sun. The first one is HD 190771, whose atmospheric parameters are: $T_{\text{eff}} = 5834 \pm 50$ K, $\log g = 4.47 \pm 0.03$, $M = 0.96 \pm 0.13 M_{\odot}$, $M/H = 0.14$ and $vsini = 4.3 \text{ km s}^{-1}$ (Valenti & Fischer 2005). For the synthesis of the stellar spectra, we took as starting point the closest model of the grid of Atlas9 atmospheric models ($T_{\text{eff}} = 5750$ K, $\log g = 4.5$ and $M/H = 0.0$), to then extrapolate to the exact values of T_{eff} , $\log g$ and metallicity (see for example, Castelli 2005).

The synthesis of the spectra covered a wavelength range of 369-1010 nm in steps of 1 km s^{-1} . As mentioned in Paper I, when constructing the MZSs our only criteria for the line selection is a minimum ratio of line-depth to continuum, which for this work we have fixed > 0.1 , resulting in a total number of individual lines of 23 172. The established MZS for the intensity, circular polarisation and null profiles are shown Fig. 9.

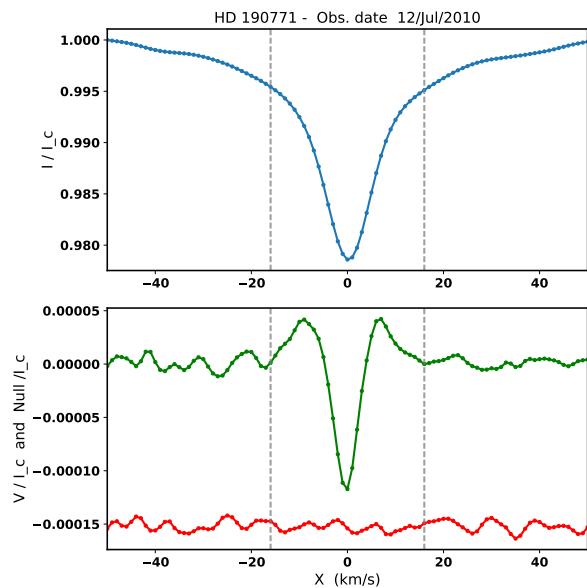


Fig. 9. From top to bottom, MZS profiles in intensity, circular polarisation and null in the reference frame of the star. The central region, determined by the vertical lines, defines the rotational span velocities for this star in the doppler space, from -16 to 16 km s^{-1} .

The next step is to fit the observed broadening for the intensity Stokes profile. For this propose, we set as free parameters the projected rotational velocity of the star ($vsini$) and the microturbulence velocity (ξ): We calculated a sample of 50 stellar spectra varying $vsini=[0.5,10]$ and $\xi=[0,5] \text{ km s}^{-1}$. We then trained an algorithm to predict simultaneously both parameters, obtaining as best fit values $vsini = 5.97$ and $\xi = 2.49 \text{ km s}^{-1}$. In Fig. 11 we show the obtained fit of synthetic profile to the observed one. In the adjustment of the intensity MZS profile, we are considering that all the other broadening processes such as the magnetic,

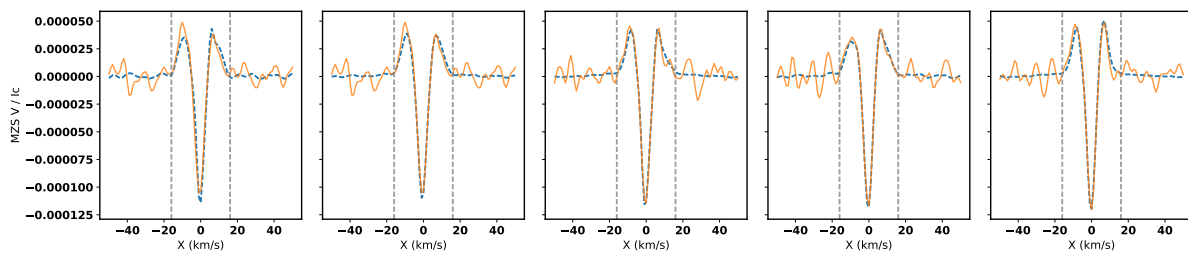


Fig. 10. Examples of MZS profiles obtained for the HD 190771 data (solid lines) and the respective denoised MZSs (dashed lines). The shape variations of the MZSs are similar to those in the synthetic case showed in the upper panel of Fig. 5. The dashed vertical lines determine the region employed in the inversion of the MZS profiles.

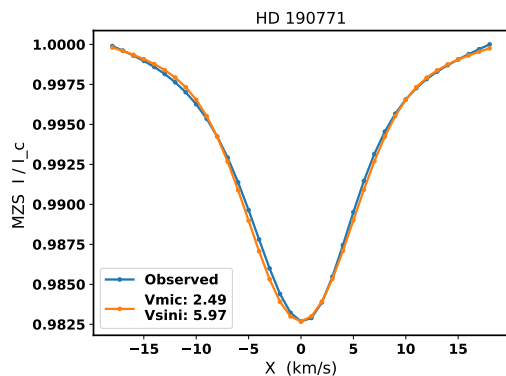


Fig. 11. MZSs in intensity for the data and the best fit model considering as free parameters v_{sini} and ξ (both in units of km s^{-1}).

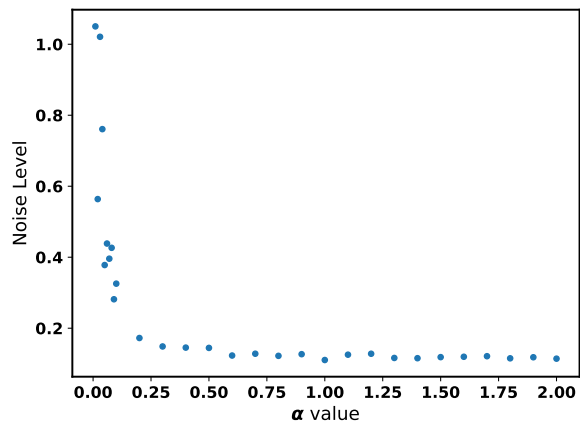


Fig. 12. Variation of the noise level of the MZSs as function of the α value used in Ec. (13); see text for details.

instrumental or macroturbulent ones, can be well represented by the interplay between only these two free parameters. For this reason, the values of v_{sini} and ξ derived from this fitting are not real *measurements* of these two physical parameters.

In summary, we use an optimal atmospheric model ($T_{\text{eff}} = 5834 \text{ K}$, $\log g = 4.47$, $M/H = 0.14$, $v_{\text{sini}} = 5.97 \text{ km s}^{-1}$ and $\xi = 2.49 \text{ km s}^{-1}$) to synthesize a set of 300 MZS that we will use to train the regression algorithms and to subsequently determine H_{eff} for this star.

In order to follow a consistent MZSs inversion procedure with our previous tests, it is required to determine the standard deviation of both, the noise-free MZS (σ_{MZS}) and the noise (σ_{noi}). The latter was determined using the edges of the circular MZS profile –indicated by the dashed vertical lines in Fig. 9–, because in these regions there is only noise. For the former, we considered only the central region where is present the polarised signature. We then applied a noise cleaning process to the polarised MZS as described in the precedent section. Once we have obtained the cleaned MZS, we calculated the standard deviation from this noise-free profile. Finally, the noise level is determined as before, $\text{NL} = \sigma_{\text{noi}} / \sigma_{\text{MZS}}$, obtaining a value of 0.15.

In order to apply the iterative inversions procedure, in each of the 39 echelle orders we added random white noise to the observed circular polarised spectra. The amplitude (A_i) of the added noise in each order is different, and it is given by :

$$A_i = \sigma_i^y / \alpha, \quad (13)$$

where σ_i^y is the standard deviation of the circular polarised spectra in the i -order, and α is a constant factor for all orders. It is

through the value of α that the NL can be controlled in the MZS after the addition of random white noise. In Fig. 12 we show how the noise level of the MZSs varies as function of the α value for this particular observation of HD 190771: For very low values of α –corresponding to high amplitudes in the added noise–, the NL is very high, but as α increases the NL decays very fast, to finally become stable at around $\text{NL} \sim 0.15$, which correspond to the noise level of the MZS when no noise was added. In this plateau phase of the NL, corresponding to α values from 0.3 to 2, we are interested in the minimum ($\alpha = 0.3$), because the lower is the value of α the higher will be the added noise, i.e., the higher will be the variations in the iterative establishment of MZS profiles. In Fig. 10, we show some examples of the of MZS profiles for the HD 190771 data considering $\alpha = 0.3$.

Finally, we considered 3 000 iterations to produce the histogram of the inversions results. In Fig. 13 we show the distribution of the inversions, as well as the fit of the normal Gaussian distribution, from which we derived a value of $H_{\text{eff}} = -6.3 \pm 0.3 \text{ G}$. Using the same dataset, Marsden et al. (2014) have reported a value of $H_{\text{eff}} = -9.8 \pm 0.3 \text{ G}$.

The value of the error in our measurement of H_{eff} is based on the MAPE results of Fig. 8. Considering that in our inversions we employed the BR regressor and given that the noise level of the data is 0.15, it corresponds to a MAPE close to 5%, i.e., an error of $\pm 0.3 \text{ G}$. It is worth noticing that the same error is reported by Marsden et al. (2014) despite the fact that in the inversion of the LSD profile, the authors they do not implement any noise treatment. As a reference, for the same NL of 0.15, the MAPE

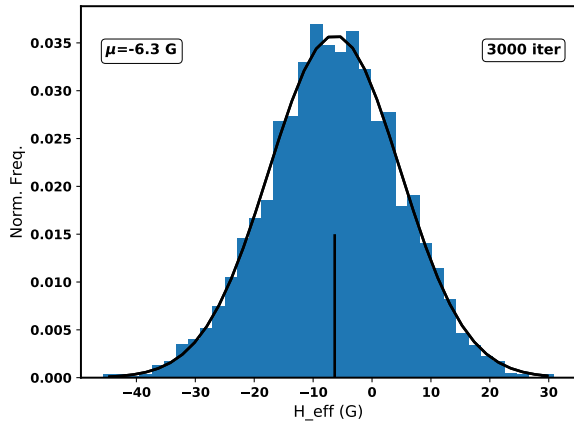


Fig. 13. Histogram of the inversions profiles for the star HD 190771, from we determined a value of $H_{\text{eff}} = -6.3$ G. The regressor algorithm employed in the inversions is the BR.

associated to *single* case (inversions without noise treatment) is 15%, i.e., the error should be around ± 1.5 G. It seems thus that the errors reported by classical techniques that do not consider noise treatment could be seriously underestimated.

Now, if we consider the estimation that we found of 1.5 G for the error in the LSD measurement of H_{eff} , then it turns out that the value of H_{eff} reported by Marsden et al. (2014) and the one we found, would be in agreement at a difference of 2σ . On the contrary, if we consider the error of 0.3 G reported by the authors, then the difference could not be explained by the uncertainties associated to the measurements, and in this case the discrepancy in the results deserve a much deeper analysis, which is beyond the scope of the present study.

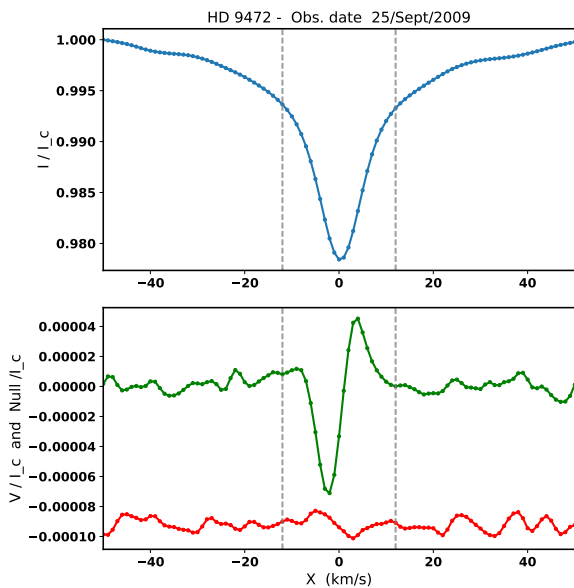


Fig. 14. Same as Fig. 9, but for HD 9472. The star spans in the doppler space from -12 to 12 km s^{-1} .

4.2. HD 9472

The second example is the star HD 9472, whose atmospheric parameters are $T_{\text{eff}} = 5867 \pm 44$ K, $\log g = 4.67 \pm 0.02$, $M = 1.29 \pm 0.19 M_{\odot}$, $M/H = 0.0$ and $v \sin i = 2.2 \text{ km s}^{-1}$ (Valenti & Fischer 2005; Marsden et al. 2014).

We have followed the same procedure as in the previous case, taking as point of departure the closest atmospheric model from the Atlas9 grid, namely, $T_{\text{eff}} = 5750$ K, $\log g = 4.5$, and $M/H = 0.0$, to then extrapolate to the exact values of T_{eff} and $\log g$. Adopting the same threshold of the line-depth to continuum as before (> 0.1), the total number of individual lines is 23 895 for this star. We then established the MZSs, shown in Fig. 14.

The next step was to reproduce the observed broadening in the intensity Stokes MZSs. We obtained as best fit values $v \sin i = 5.08$ and $\xi = 1.81 \text{ km s}^{-1}$, which produced, as in the precedent case, a very good fit between the synthetic and the observed profiles, as showed in Fig. 15.

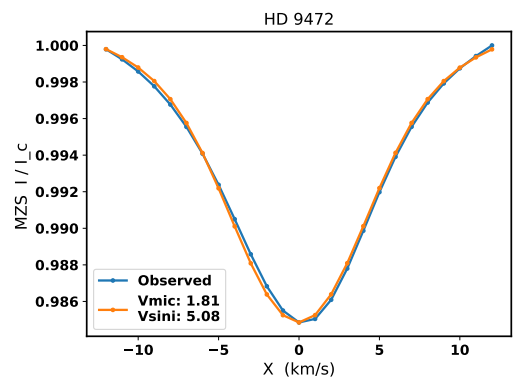


Fig. 15. Same as Fig. 11, but for HD 9472.

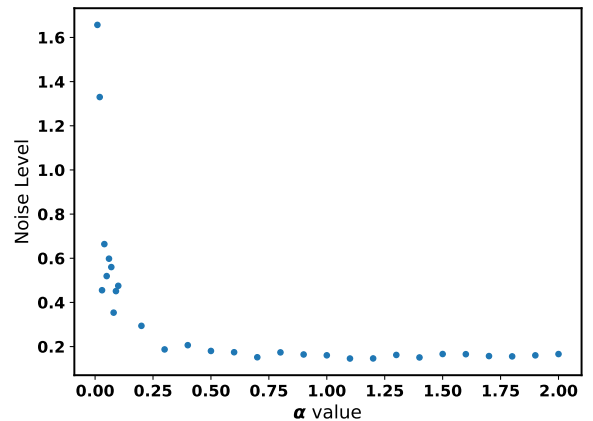


Fig. 16. Same as Fig. 12) but for the data of HD 9472.

The NL was then calculated for the circular MZS, obtaining a value of 0.19. We subsequently inspected the variation of the noise level as function of the amplitude of the random noise added to the echelle orders, allowing to determine that setting $\alpha = 0.4$ will correspond to MZSs with the same NL as the original data of 0.19, see Fig. 16. Finally, we iteratively established 3 000 MZSs to consequently fit a Gaussian distribution to the histogram of the inversions, shown in Fig. 17. The centroid of the

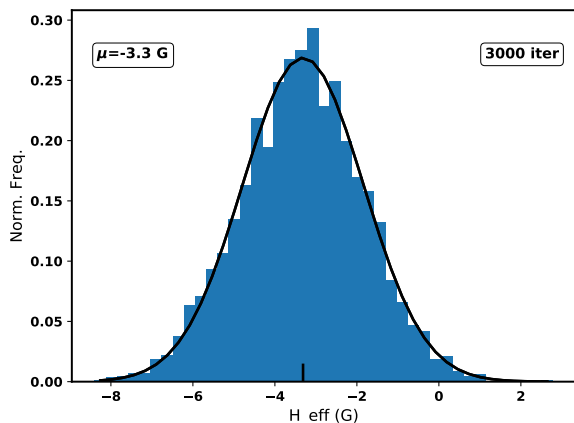


Fig. 17. Histogram of the inversions profiles for the star HD 9472, from we determined a value of $H_{\text{eff}} = -3.3$ G. The regressor algorithm employed in the inversions is the BR.

fitted distribution corresponds to a value of $H_{\text{eff}} = -3.3 \pm 0.2$ G, which in fact is almost the same that the one reported by Marsden et al. (2014) using the same data: $H_{\text{eff}} = -3.5 \pm 0.4$ G. Once more, it seems that the error reported by the authors is underestimated: based in Fig. 8, for this noise level the error should be around 17%, i.e., 0.6 G.

5. Conclusions

We have presented a new study related to the measurement of stellar longitudinal magnetic fields, from high resolution spectropolarimetric data, analysing multi-line profiles. Our main goal was to develop a general method which is constrained nor by the regime of validity of the weak field approximation neither by the line autosimilarity normally assumed in the classical methods employed nowadays in the measurement of H_{eff} .

Our technique is thus based on a theoretical radiative transfer approach where we produced a synthetic set of Stokes profiles, each one corresponding to a different configuration of the magnetic fields over the stellar surface. Considering the best possible scenario of noise-free spectra, we have showed that the use of machine learning algorithms (MLA) is a key step to reduce the number of synthetic profiles required for an acceptable accuracy in the correct determination of H_{eff} : With the use of MLA and considering only 50 stellar spectra, we obtained a better value of the RMSE for the inversion results that when we considered 7 500 spectra but the inversion strategy was based in a look-up table, i.e., no MLA was applied (Ramírez Vélez et al. 2016).

We also showed that the results are considerably degraded when noise is included; nevertheless this is not restricted to the MLA but in general to any method dealing with the inversion of noise-affected profiles or signals. We thus proposed a data noise pre-processing consisting of two steps: 1) To use PCA to perform a noise-cleaning of the multi-line profiles and 2) An iterative inversion procedure. Applying this data analysis process, we achieved a considerable improvement in the inversion accuracy, confirming that it is desirable to include a noise treatment in the analysis of multi-line profiles in order to get more confidence in the derived values of H_{eff} . Very similar results about the impact of the noise in the inversion of multi-lines profiles were independently found by Carroll & Strassmeier (2014).

We implemented our inversion technique to real observations of two stars. In order to similarly apply the MLAs to the observed data set (i.e. as closely as possible as in the case of synthetic spectra), it was first required to reproduce the observed broadening in the intensity profile. We allowed the variation of two physical parameters for this propose, namely, $v \sin i$ and ξ , and we obtained very good fits, as shown in Figs. 11 and 15. Of course, the values of these two parameters lack of any physical interpretation because we are assuming that all other broadening mechanisms (e.g. magnetic, instrumental or any other) can be well represented by considering only $v \sin i$ and ξ as adjustable parameters.

Thus, the atmospheric model employed for the analysis of each star consisted in the exact values of T_{eff} , $\log g$ and metallicity –reported by other authors–, in addition to the values of $v \sin i$ and ξ . Once these five atmospheric parameters were defined, we synthesized a set of 300 polarised stellar spectra that in turn were used to train the MLA (the used training data sets can be found in www.astrosen.unam.mx/~julio/ML_mzs). One final step was to reproduce the iterative inversions methodology implemented in the synthetic tests. For this purpose, we added random white noise in each order of the echelle spectrum. The amplitude of the added noise in each order is different and is controlled by one free parameter, labelled α in Eq. (13). It is through the value of this parameter that it was possible to keep a constant noise level in the MZSs established for the iterative inversions. Finally, considering the same number of iterations in the case of real data than in the tests, we fitted a Gaussian normal function to the distribution of the inversion results. The centroid of the Gaussian distribution determines the value of H_{eff} for each data set (Figs. 13 and 17).

We have used two stars as test cases to illustrate the direct application of the proposed methodology to real observations, and in this sense, it is not the scope of this work to compare the measured values of H_{eff} with our technique with the ones obtained by other methods. We will proceed to the comparison of the values of H_{eff} obtained with classical methods versus ours in a forthcoming article. However, what we can highlight the fact that the uncertainties reported in the measurement of H_{eff} from the LSD profiles are most likely underestimated. Asensio Ramos & Petit (2015) have recently presented a method to establish and analyse LSD profiles under a Bayesian framework. One of the advantages of this approach is that it can estimate the intervals of credibility at each velocity point of the LSD profiles. Unfortunately, although the authors applied their method to three different stars, they did not report the respective measurements of H_{eff} , preventing the comparison of their estimation of errors with other techniques. As far as we know, no other work has addressed a detailed study on the expected uncertainties associated to the measurements of H_{eff} from noise-affected LSD profiles.

The most relevant aspect of the work presented here is not that we have included estimations of the uncertainties in the measurements of H_{eff} , but the fact that we have introduced a new methodology for the analysis of polarised multi-line profiles –including a radiative transfer theoretical framework in the synthesis of the Stokes profiles–, using a strategy based on machine learning algorithms. We expect to apply our data analysis method to stars other than solar-type stars in incoming studies.

Acknowledgements

We are very grateful to the whole group of *Laboratorio de Computo Inteligente del CIC-IPN*² for very constructive and illustrative discussions about machine learning methods. We would also like to express our acknowledgement to the anonymous referee for all the comments that helped to improve the clarity of this work. JRV acknowledges support grants from CONACYT 240441 and SUPERCOMPUTO – LANCAD-UNAM-DGTIC-326. Thanks go to AdaCore for providing the GNAT GPL Edition of its Ada compiler.

References

- Angelou, G. C., Bellinger, E. P., Hekker, S., & Basu, S. 2017, *ApJ*, 839, 116
- Armstrong, D. J., Kirk, J., Lam, K. W. F., et al. 2016, *MNRAS*, 456, 2260
- Asensio Ramos, A. & de la Cruz Rodríguez, J. 2015, *A&A*, 577, A140
- Asensio Ramos, A. & Petit, P. 2015, *A&A*, 583, A51
- Bellinger, E. P., Angelou, G. C., Hekker, S., et al. 2016, *ApJ*, 830, 31
- Carlin, B. P. & Louis, T. A. 2008, *Bayesian methods for data analysis* (CRC Press)
- Carroll, T. A. & Strassmeier, K. G. 2014, *A&A*, 563, A56
- Castelli, F. 2005, *Memorie della Societa Astronomica Italiana Supplementi*, 8, 25
- Castelli, F. & Kurucz, R. L. 2004, *ArXiv Astrophysics e-prints* [astro-ph/0405087]
- Chang, C.-C. & Lin, C.-J. 2011, *ACM transactions on intelligent systems and technology (TIST)*, 2, 27
- Davies, G. R., Silva Aguirre, V., Bedding, T. R., et al. 2016, *MNRAS*, 456, 2183
- Donati, J.-F. & Landstreet, J. D. 2009, *ARA&A*, 47, 333
- Donati, J.-F., Semel, M., Carter, B. D., Rees, D. E., & Collier Cameron, A. 1997, *MNRAS*, 291, 658
- Du, K.-L. & Swamy, M. 2014, in *Neural Networks and Statistical Learning* (Springer), 15–65
- García-Florián, A., López-Martín, C., Yáñez-Márquez, C., & Abran, A. 2018, *Information and Software Technology*
- Glantz, S. A., Slinker, B. K., & Neillands, T. B. 2016, *Primer of applied regression & analysis of variance* (McGraw-Hill Medical Publishing Division)
- Golub, G. H. & van Loan, C. F. 1996, *Matrix computations*
- Grunhut, J. H., Wade, G. A., Neiner, C., et al. 2017, *MNRAS*, 465, 2432
- Jefferies, J., Lites, B. W., & Skumanich, A. 1989, *ApJ*, 343, 920
- Kochukhov, O., Makaganiuk, V., & Piskunov, N. 2010, *A&A*, 524, A5
- Marsden, S. C., Petit, P., Jeffers, S. V., et al. 2014, *MNRAS*, 444, 3517
- Mathys, G. 1989, *Fund. Cosmic Phys.*, 13, 143
- Paletou, F. 2012, *A&A*, 544, A4
- Pedregosa, F., Varoquaux, G., Gramfort, A., et al. 2011, *Journal of Machine Learning Research*, 12, 2825
- Petit, P., Dintrans, B., Solanki, S. K., et al. 2008, *MNRAS*, 388, 80
- Petit, P., Louge, T., Théado, S., et al. 2014, *PASP*, 126, 469
- Ramírez Vélez, J. C., Semel, M., Stift, M., et al. 2010, *A&A*, 512, A6
- Ramírez Vélez, J. C., Stift, M. J., Navarro, S. G., et al. 2016, *A&A*, 596, A62
- Rees, D. E., López Ariste, A., Thatcher, J., & Semel, M. 2000, *A&A*, 355, 759
- Rees, D. E. & Semel, M. D. 1979, *A&A*, 74, 1
- Richards, J. W., Starr, D. L., Butler, N. R., et al. 2011, *ApJ*, 733, 10
- Rosenblatt, F. 1958, *Psychological review*, 65, 386
- Rumelhart, D. E., Hinton, G. E., & Williams, R. J. 1985, *Learning internal representations by error propagation*, Tech. rep., California Univ San Diego La Jolla Inst for Cognitive Science
- Schölkopf, B., Smola, A. J., Williamson, R. C., & Bartlett, P. L. 2000, *Neural computation*, 12, 1207
- Semel, M. & Li, J. 1996, *Sol. Phys.*, 164, 417
- Semel, M., Ramírez Vélez, J. C., Martínez González, M. J., et al. 2009, *A&A*, 504, 1003
- Semel, M., Rees, D. E., Ramírez Vélez, J. C., Stift, M. J., & Leone, F. 2006, in *Astronomical Society of the Pacific Conference Series*, Vol. 358, *Astronomical Society of the Pacific Conference Series*, ed. R. Casini & B. W. Lites, 355
- Sennhauser, C. & Berdyugina, S. V. 2010, *A&A*, 522, A57
- Sennhauser, C., Berdyugina, S. V., & Fluri, D. M. 2009, *A&A*, 507, 1711
- Stift, M. J. 1975, *MNRAS*, 172, 133
- Stift, M. J. 2000, *A Peculiar Newsletter*, 33, 27
- Stift, M. J., Leone, F., & Cowley, C. R. 2012, *MNRAS*, 419, 2912
- Tan, P.-N., Steinbach, M., & Kumar, V. 2005, *Introduction to data mining* (Pearson Addison Wesley), 769
- Valenti, J. A. & Fischer, D. A. 2005, *ApJS*, 159, 141
- Vapnik, V. N. 1999, *IEEE transactions on neural networks*, 10, 988
- Verma, K., Hanasoge, S., Bhattacharya, J., Antia, H. M., & Krishnamurthi, G. 2016, *MNRAS*, 461, 4206
- Wade, G. A., Donati, J.-F., Landstreet, J. D., & Shorlin, S. L. S. 2000, *MNRAS*, 313, 823
- Wade, G. A., Neiner, C., Alecian, E., et al. 2016, *MNRAS*, 456, 2
- Yang, Y. & Zou, H. 2015, *Statistics and Computing*, 25, 1129

² <http://www.cic.ipn.mx/sitioCIC/index.php/pre-rcnc>

Appendix A: Hyperparameters for each regressor

For the definition of each of the hyperparameters listed below, we refer the reader to *Scikit-learn* user guide. For consistence, we labeled each parameter following the mentioned guide ³.

Appendix A.1: Bayesian Ridge

```
BayesianRidge(alpha_1=1e-06, alpha_2=1e-06, compute_score=False, copy_X=True, fit_intercept=True, lambda_1=1e-06, lambda_2=1e-06, n_iter=300, normalize=False, tol=0.001, verbose=False)
```

Appendix A.2: Artificial Neuronal Network

```
MLPRegressor(activation='identity', alpha=0.05, batch_size='auto', beta_1=0.9, beta_2=0.999, early_stopping=False, epsilon=1e-08, hidden_layer_sizes=(100,), learning_rate='constant', learning_rate_init=0.001, max_iter=10000, momentum=0.9, nesterovs_momentum=True, power_t=0.5, random_state=25, shuffle=True, solver='lbfgs', tol=1e-08, validation_fraction=0.1, verbose=False, warm_start=False)
```

Appendix A.3: Support Vector Machine

```
SVR(C=50.0, cache_size=200, coef0=0.0, degree=3, epsilon=0.1, gamma='auto', kernel='linear', max_iter=-1, shrinking=True, tol=0.001, verbose=False)
```

³ http://scikit-learn.org/stable/_downloads/scikit-learn-docs.pdf